Frame Design for Adaptability in Long-Range Underwater Communication

Michel Barbeau[1(✉)], Stéphane Blouin[2], and Ahmad Traboulsi[1]

[1] Carleton University, Ottawa, ON, Canada
barbeau@scs.carleton.ca
[2] Defence R&D Canada, Atlantic Research Centre, Dartmouth, NS, Canada

Abstract. The problem addressed in this paper is adaptable long range underwater acoustic communications. We use low frequency underwater acoustic waves that have potential for long range communications. Underwater propagation conditions can vary considerably. We define protocol elements for adaptable underwater communications. They comprise six frame formats with a wide range of robustness with respect to the underwater communication conditions. We vary the interval of symbols of 4-tone Frequency-Shift Keying modulation from one format to another. This has the effect of increasing the SNR. Hence, the ability to operate in less favorable conditions. The performance of our design is evaluated through simulation.

Keywords: Underwater communications · Weak signal communications · Arctic · Software-defined communications

1 Introduction

The underwater environment is a relatively new data communication challenge. The need for underwater communication is related to applications such as monitoring and surveillance of coastal waters [21], submarine activity sensors [22], autonomous undersea vehicles [10], underwater robots [7] and submerged airplane locator beacons [29].

In this paper, we focus on low frequency acoustic communications [11,16]. We aim at long-range underwater acoustic communications that are robust to environmental changes. They are critical for wide-area surveillance systems developed for the Canadian Arctic [12]. Recent studies [13] tend to demonstrate that underwater communications in high frequencies ranges can reach up to 10-to-20 km with reasonable power levels. In contrast to high frequencies, Stojanovic has

This work was supported by the Public Works and Government Services Canada under Contract No. W7707-216847/001/HAL through the Defence Research and Development Canada.

W. Bao et al. (Eds.): ADHOCNETS 2021/TridentCom 2021, LNICST 428, pp. 130–143, 2022.
https://doi.org/10.1007/978-3-030-98005-4_10

pointed out that attenuation is lower in low frequencies [26]. The potential for very-long distance transmissions in low frequencies has been established [15].

In our research, we focus on the acoustic 200 Hz to 2 kHz frequency band for long-rang underwater communications. We also acknowledge that the narrow half-power bandwidth, associated with low underwater acoustic frequencies and long distances, limits applications to low data rates. In Refs. [1–4,8,18,19], we describe the design of a physical and frame layer protocol for long range underwater communications. In a recent companion paper, we have been able to show that we can achieve source-receiver separation distances well above 30 km in the Canadian Arctic environment [9]. The goal of the research presented in this paper is to improve the robustness of our communication system. We aim to achieve much larger source-receiver separation distances (in the order of 100-to-500 km) and introduce adaptability to environmental changes (such as variations in the nature or magnitude of noise, ice presence, and sound speed profile). The intention is to realize a design that can achieve long-range communications in the Canadian Arctic environment, in all seasons.

In this paper, we define six frame formats with increasing degree of robustness. Our strategy is to increase robustness by augmenting the Signal-to-Noise Ratio (SNR), in particular the energy contained in every 4-tone Frequency-Shift Keying (4-FSK) symbol. The performance of the six frame formats is characterized through simulation. Building on these six frame formats, we define adaptability protocols to variable underwater propagation conditions.

Related work is reviewed in Sect. 2. The underwater communication system design is reviewed in Sect. 3. The design of the receiver is outlined in Sect. 4. Its Matlab™ implementation is discussed in Sect. 5. Performance evaluation results are presented in Sect. 6. The adaptability protocols are specified in Sect. 7. Section 8 concludes the paper.

2 Related Work

Song et al. emphasized that one of the key underwater communication issues is adaptability to changing propagation conditions [25]. Most of the adaptability techniques rely on the use of feedback returned by the receiver to the source to dynamically adapt transmission parameters, such as modulation or Forward Error Correction (FEC) [5,6,24,28].

In this paper, we adapt the SNR to the propagation conditions. The SNR is defined as the following equation:

$$SNR = \frac{P}{N} = \frac{E_b R}{B N_0} \tag{1}$$

This equation tells that the SNR is equal to the ratio of the signal power (P) over the channel noise power (N). In turn, the signal power is equal to the product of the energy per bit (E_b) times the data rate (R). While the channel noise power is equal to the product of the channel bandwidth (B) times the noise power spectral density (N_0). It is a well-established fact that augmenting the SNR increases the

robustness of communications [23]. Indeed, higher SNR does achieve better Bit Error Rate (BER) and Frame Error Rate (FER). To increase the SNR, we can either augment the values of the numerators E_b or R or lower the values of the denominators B or N_0. The noise power spectral density is function of the environment. The transmission power, hence the quantity E_b, can be cranked up at the expense of energy consumption. The transmission power is constrained by the capabilities of the equipment. The bandwidth can be narrowed. We do use a very narrow bandwidth signal already (4.4 Hz). In this paper, we make the choice of lengthening the time interval of symbols to improve robustness of underwater communications. The data rate R is reduced. For a given power level P, there is more energy in every bit (E_b). The bit SNR (E_b/N_0) is augmented, proportionally to the reduction of R.

Table 1. Frame formats of the six communication modes.

Mode	T (sec.)	F (sec.)	R (bps)	Efficiency	k	Samples/ symbol	FFT bin width (Hz)
1 min	0.34	55.30	0.90	0.21	1	128	1.46
2 min	0.68	110.59	0.45	0.10	2	256	0.73
4 min	1.37	221.18	0.23	0.05	4	512	0.37
8 min	2.73	442.37	0.11	0.03	8	1024	0.18
16 min	5.46	884.74	0.06	0.01	16	2048	0.09
20 min	6.83	1105.92	0.05	0.01	20	2560	0.07

3 Communication System Design

To support various underwater communication propagation conditions, we define six different modes of communications. Every mode has a corresponding frame format. Table 1 shows key design parameters for every format.

The formats have common and specific parameters. For all modes, every frame comprises 162 channel symbols that encode 50 data bits. Convolutional FEC of the data bits yields 162 code bits. Every code bit is paired with a synchronization bit. Each pair makes a channel symbol. The 4-FSK complex modulation envelope frequencies are -2.2, -0.73, 0.73 and 2.2 Hz, corresponding to the channel symbols 11, 10, 01 and 00. The signal bandwidth is 4.4 Hz. Every mode has a specific symbol time interval (T) and, consequently a specific frame interval (F), the second and third columns in Table 1. The value of the third column results from the product of the number of symbols (162) time the symbol time interval. For each frame format, the fourth column shows the achieved effective data rate (the ratio $50/F$). Defining the bandwidth efficiency as the ratio effective data rate over bandwidth, (the ratio $R/4.4$), the fifth column shows the bandwidth efficiency for every mode.

In previous papers, we described several aspects of our communication system design. [1–4,8,18,19]. In the sequel, we focus on the aspects that are new and

required for the support of the six frame formats. We also briefly summarize the mechanisms that have been described in our previous papers.

3.1 Physical Layer: 4-FSK

We use 4-FSK modulation, a specific kind of Multiple Frequency-Shift Keying (MFSK). Orthogonality of MFSK symbols is guaranteed when the frequency separation between symbols Δf is equal to the ratio $k/(2T)$, for a positive integer k (see Ref. [20], P. 110). As a function of the supported mode, the sixth column of Table 1 shows the value of the positive integer k. The resulting frequency separation between symbols and signal bandwidth are the same for all modes, i.e., 1.46 and 4.4 Hz. Despite the fact that six different frame formats are defined, solely on type of modulation needs to be supported. This simplifies the implementation.

4 Receiver Design

The receiver uses a common sampling rate for all supported modes, 375 samples per second. It means, that 187 Hz of signal bandwidth is simultaneously processed. The receiver searches for frames in a frequency domain representation of the signal bandwidth. This achieves an auto tune capability that can deal with frequency drifts due to Doppler effects and source-receiver miss frequency alignments.

4.1 Frequency Domain Representation

The seventh column of Table 1 shows the number of samples per symbol for every mode. The receiver constructs a frequency domain representation of the signal bandwidth using the Fast Fourier Transform (FFT). Every FFT spans the duration of two symbols. The eight column of Table 1 provides for every mode the FFT bin width (Hertz). The bin width is calculated dividing the sample rate by two times the number of samples per symbol.

Using the frequency-domain representation, candidate frequencies are identified as the presence of local Signal-to-Noise Ratio (SNR) peaks and correlation with the bit synchronization pattern. To find the peaks, the smoothed average magnitude level at each frequency bin is calculated. The magnitude is smoothed taking, for each frequency, the sum of the magnitudes of signals within the signal bandwidth (4.4 Hz). The frequency domain representation is normalized with respect to the noise level. The smoothed representation of the spectrum yields candidate frequencies, that is, signal peaks with potential frames. Candidate frequencies are examined to evaluate correlation with the 162-bit synchronization pattern. There is correlation when there is consistently energy peaks at signal positions corresponding to synchronization bits. When a correlation with the bit pattern is confirmed, candidate frequencies are analyzed deeper. Following that second frequency-domain analysis, relevant parameters are obtained that include the estimated time shift (relative to the sample window start) and SNR. The next step resolves time delays and demodulate the signals at the candidate frequencies.

4.2 Soft Symbol Calculation

We use Fano sequential decoding of convolutional codes [14,17]. It is sub-optimal, but it can process codes with long coding sequences, 32 bits in our case. Fano sequential decoding requires the calculation of soft symbols. We explain how we calculate soft symbols. Let $x_0, x_1, \ldots, x_{n-1}$ represent the discrete complex samples of channel data. In 4-FSK, at every symbol position there are four possible symbol values. For every of the four 4-FSK possibilities, the power of the signal at every position is calculated. Over a symbol interval of length T, signal samples x_t correlated with the waveform values $e^{-j2\pi ft}$ are added together to obtain the total signal magnitude at every symbol frequency, $i = 0, \ldots, 161$ and $f = -2.2, -0.73, 0.73, 2.2$:

$$P_{i,f} = \left| \sum_{t=iT+\tau}^{(i+1)T+\tau-1} x_t \cdot e^{-j2\pi ft} \right|$$

This calculation of cumulative power is represented in the diagram of Fig. 1.

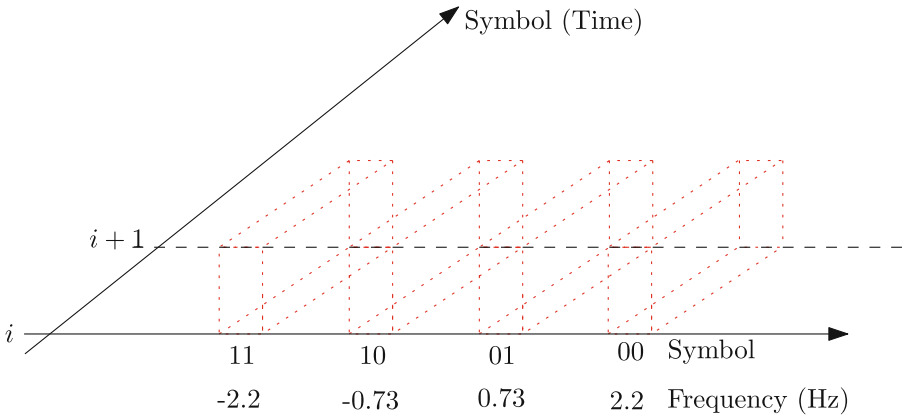

Fig. 1. At symbol position i, cumulative power for every of the four 4-FSK possible symbols (red-dotted line delimited). (Color figure online)

The corresponding channel symbols, in binary, are also shown, 00, 01, 10 and 11. Every box, delimited by red dotted lines, represents a frequency-symbol-amplitude space where sample values x_t for symbol i are correlated with waveform values $e^{-j2\pi ft}$ and summed up resulting into a magnitude denoted as $P_{i,f}$. For every channel symbol, note that the most significant bit is the data bit while the least significant bit is the synchronization bit.

For every symbol index i, soft symbol σ_i is calculated, according to the value of synchronization bit at position s_i:

$$\sigma_i = s_i \cdot (P_{i,2.2} - P_{i,-0.73}) + \neg s_i \cdot (P_{i,0.73} - P_{i,-2.2}) \quad (2)$$

When the synchronization bit (s_i) is one, the term $P_{i,2.2} - P_{i,-0.73}$ represents the difference of power at the symbol corresponding to data bit one versus the power at the symbol corresponding to data bit zero. The term $P_{i,0.73} - P_{i,-2.2}$ does the same when the synchronization bit at position i is a zero. A positive σ_i value proportionally indicates that the symbol at position i is a one, whereas a value of σ_i in the negative indicates proportionally, in the negative direction, that it is a zero. A near-zero σ_i corresponds to an ambiguous symbol.

The soft symbol σ_i is mapped to a normalized score z_i. Let SD denote the standard deviation of the 162 soft symbols. The score z_i expresses soft symbol σ_i in scaled units of standard deviation SD, that is:

$$z_i = 50\frac{\sigma_i}{SD} \tag{3}$$

The multiplicand 50 is the scaling factor. When the standard deviation SD is null, the score z_i is equal to the product $50\sigma_i$. Finally, every score is mapped in the $[1, 256]$ interval, adding value 129 to each of them. Figure 2 shows the scores obtained in non-noisy conditions (standard deviation is 265.55). Binary value zero is scored 79, while binary value one is scored value 179. Figure 3 shows the scores obtained in noisy conditions, with a 2.5 kHz SNR of -27 dB (standard deviation 30.02). The lowest values represent the most definite binary zeros, while the highest values represent the most definite binary ones. Finally, every score z_i is mapped to a quality metrics q_i. Figure 4 shows the quality metrics versus the scores. Small scores correspond to good quality zeros or poor quality ones, while it is the opposite for high scores. While the search is conducted for mapping channel symbols to data bits, quality symbols are tried first. When the decoding fails, alternative decoding with lower quality symbols is attempted.

5 Matlab Implementation

Using the Matlab™ app designer, the Oceanus application has been developed. It supports all communication modes explained in this paper. Using the interface, the user has the option of choosing one of the available six frame formats (Table 1). The interface comprises two panels, see Fig. 5. The first panel is for the transmitter. It contains the option of typing hexadecimal data or generating random frames. The user also has the option of choosing the output device and carrier frequency. Moreover, quiet time, sampling rate and the type of output file are options the user can pick. The transmitter enables the user to either play signals directly to output devices or to save to files, giving the option to replay signals with many of the available audio applications. For simulation purposes, the user can add white noise to signals and generate signals with different SNRs. Oceanus also supports generating a probe signal. The probe signal can be used for adaptability. The user can choose frequency, sampling frequency, and file type in case the user chose to save the signal. The probe signal consists of six frames each in a different mode. Starting with mode 1 up to mode 6. The second panel is dedicated to the receiver. The user can click start the receiving state. The

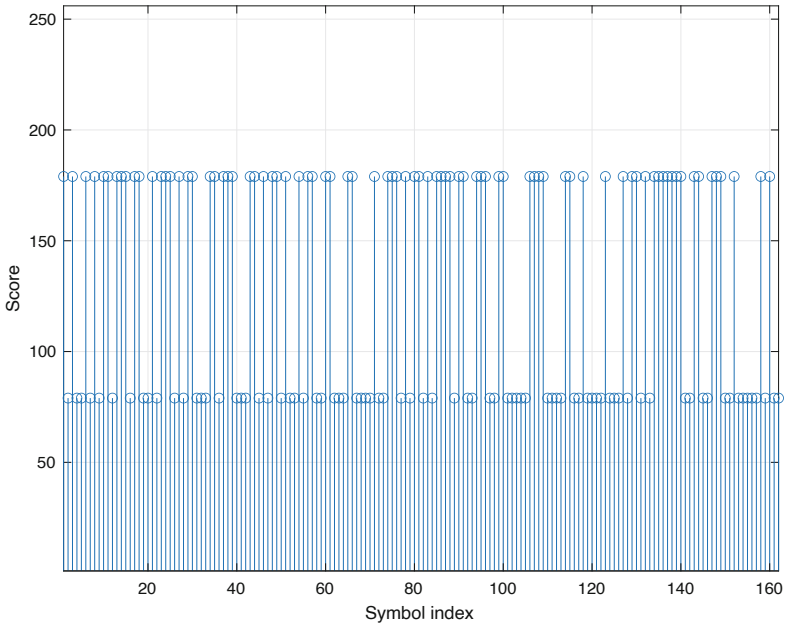

Fig. 2. Non-noisy symbol scores.

application starts listening for frames through the chosen input device. The user may choose the carrier and sampling frequencies. Oceanus provides the option of decoding in real-time from an input device or from files, in various audio formats (WAV, FLAC, OGG or MP4). Moreover, the receiver also supports adaptability. In the receiver panel, the start probe mode button would make the receiver start listening and try decoding the received signal using all the six modes in order to find the best mode. The code of the application is available online [27].

6 Performance Evaluation Through Simulation

Figure 6 shows the FER versus SNR obtained through simulation for every frame format described in Table 1. Every data point is the average of 10 trials. For this simulation, the reference bandwidth is 6 kHz. A frame is considered error-free when it is transmitted and received with no bit error. When a frame contains one or more errors, the whole frame is in error. To obtain the target SNRs, white Gaussian noise is added to the signals. Every frame format exhibits a waterfall behavior, that is, an abrupt transition from a 100% to a null FER. This is a well-known phenomenon associated with convolutional coding. From the *one minute* to the *20 min* formats, there is increase in robustness, that is, the ability to equally perform with a three dB drop SNR, from one format to another. Simulation results confirm the expected relative performance from one format to another. The symbol interval time, energy and SNR, in linear form

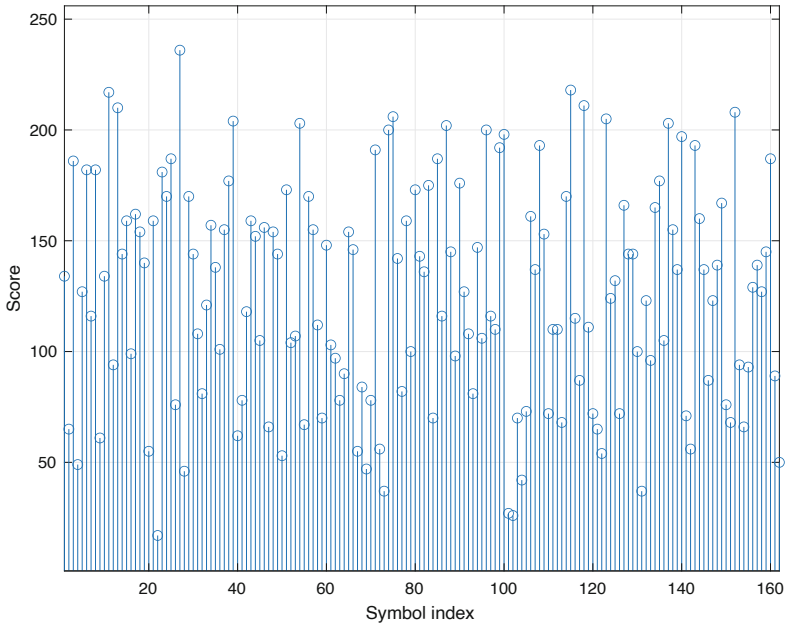

Fig. 3. Noisy symbol scores.

are consistently multiplied by two from one format to the other. From the two minutes to the 20 min mode, the crest of the waterfall is shifted −10 dB, which is consistent with the fact that symbols contain 10 times more energy.

7 Adaptability

In this section, we discuss adaptability to propagation conditions leveraging the six frame formats defined in Sect. 3. Three two-way handshake protocols are outlined to select between two peers, an Initiator and a Responder, a frame format suitable to the propagation conditions. The goal is to select the less robust frame format that can be supported, since it is also the most efficient. Feedback based, the protocols are half duplex, full duplex or parallel.

7.1 Half Duplex Feedback Protocol

Figure 7 illustrates the first protocol, where half-duplex communications are assumed. There is an Initiator and a Responder. The Initiator starts the execution of the protocol by sending a sequence of six frames. The frames are in the *one* to the *20 min* modes. That is from the less robust, but most efficient, to the most robust, but least efficient. The goal is to determine the most efficient format that can be supported by the propagation conditions. After each frame transmission, the Initiator remains silent for a duration corresponding to the

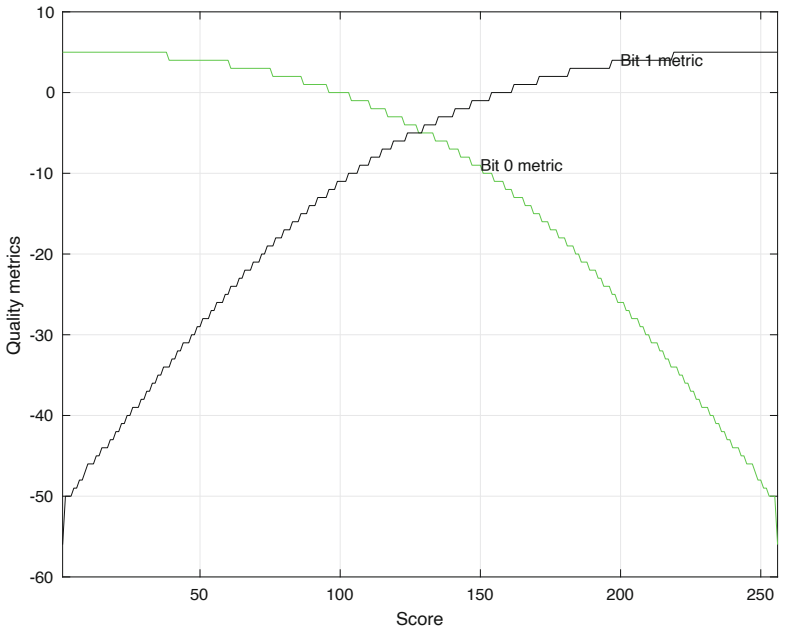

Fig. 4. Mapping of score to quality metrics.

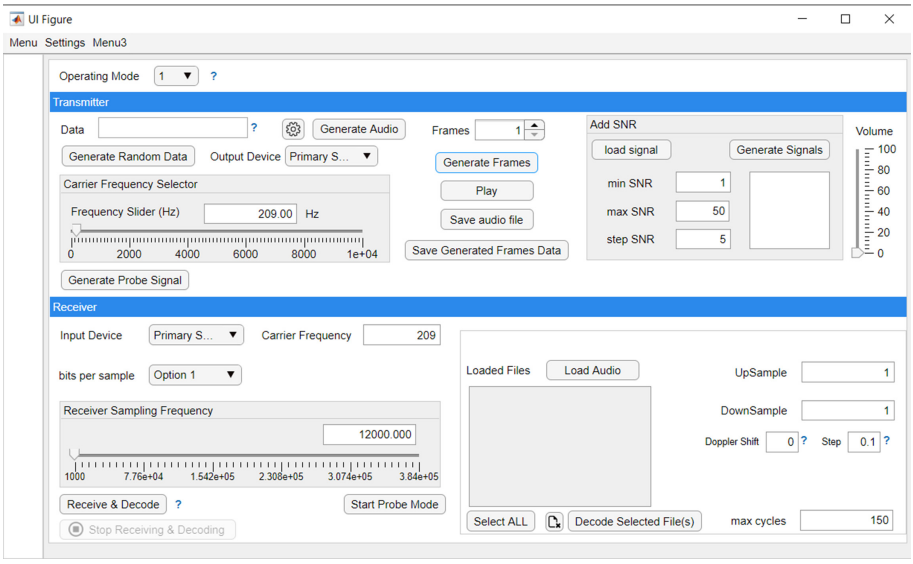

Fig. 5. Oceanus user interface.

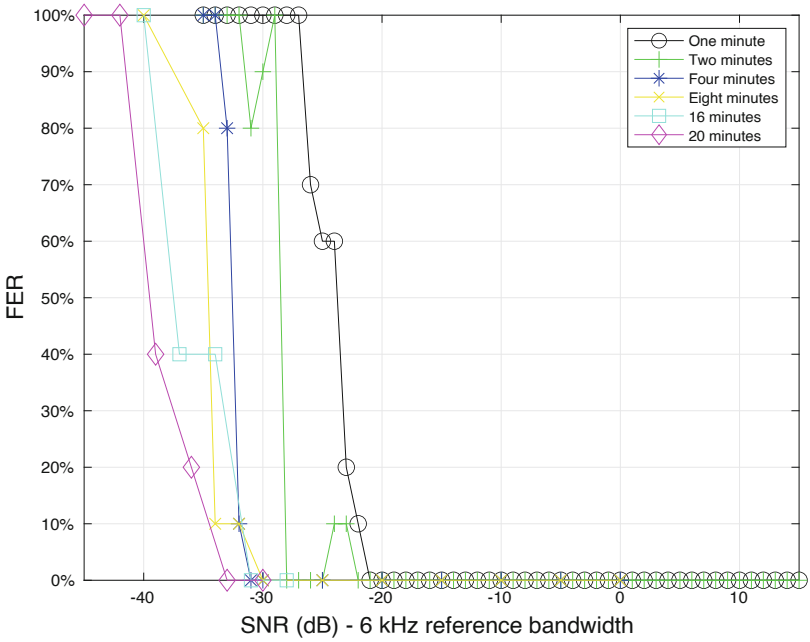

Fig. 6. FER vs. SNR.

frame time interval. It listens. In Fig. 7, at time t_1 the Initiator completes the transmission of the frame in the four minutes mode. The frame is received with success. The Responder confirms by sending a frame in the same format. From time t_2, both the Initiator and Responder continue the conversation in the *two minutes* modes. For the sake of simplicity, Fig. 7 makes abstraction of processing time and propagation delays. Symmetric propagation conditions are assumed. The Initiator and Responder can periodically repeat the handshake to update the choice of frame format to changing propagation conditions.

7.2 Full Duplex Feedback Protocol

Figure 8 illustrates the second feedback protocol, where the six supported frame formats are sent sequentially by the Initiator, one after the other from time t_0. Transmission completion is expected after a time corresponding to the sum of the time intervals all six modes. Slightly after time t_1, the Responder receives with success the frame in the *four minutes* mode. It acknowledges with a frame in the same mode. Starting from time t_2, the Initiator-Responder conversation can carry on in the *four minutes* mode.

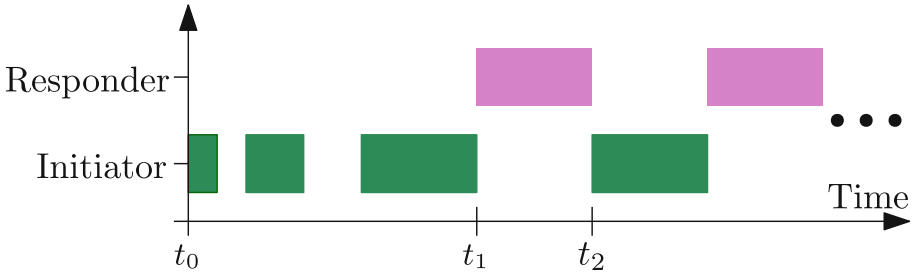

Fig. 7. Half duplex feedback protocol.

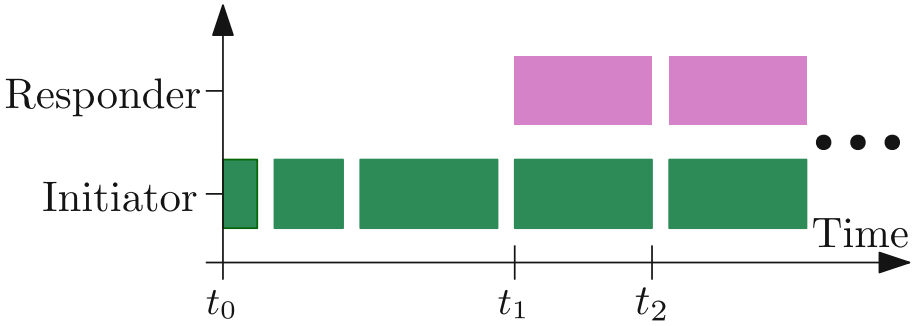

Fig. 8. Full duplex feedback protocol.

7.3 Parallel Feedback Protocol

Figure 9 depicts a third feedback protocol. At time t_0, the Initiator sends the six frame formats in parallel. Slightly after time t_1, the Responder receives with success the frame in the *four minutes* mode. It acknowledges with a frame in the same mode, reaching the Initiator at time t_2. The sequel of the Initiator-Responder conversation can carry on in the *four minutes* mode, full duplex. This feedback scheme is possible only when the Initiator and Responder have the capacity to send and receive frames in parallel.

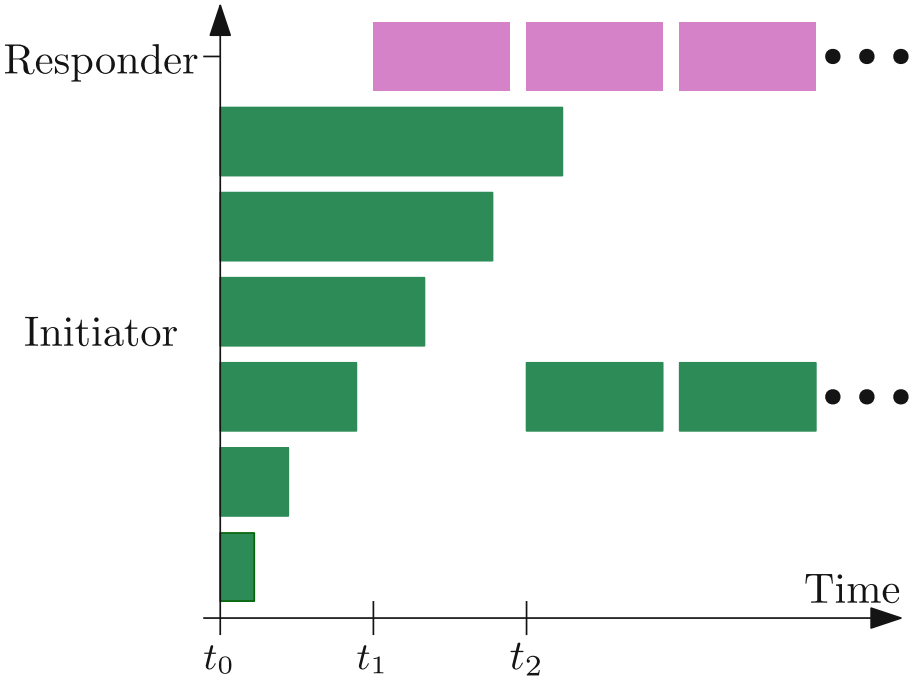

Fig. 9. Parallel feedback protocol.

8 Conclusion

We have introduced the design of six frame formats for underwater acoustic communications. The design addresses physical and link layer issues. The design has been implemented and evaluated through simulation in the Matlab™ environment. Simulation results confirm a robustness increase from one format to the other. This is due to the fact that the symbol interval is doubled from format-to-format. It has proportionally the same effect on the bit SNR, for a given transmission power level. The six formats can be used for adaptable underwater acoustic communications. We have described three adaptability protocols, that can be chosen according to available acoustic communication resources. Note that the system design does not require dynamic memory allocation anywhere. Hence, the amount of required hardware resources is predictable, in particular memory. The system design can easily be implemented on resource constrained devices.

References

1. Ahmad, A.M., Barbeau, M., Garcia-Alfaro, J., Kassem, J., Kranakis, E.: Tuning the demodulation frequency based on a normalized trajectory model for mobile underwater acoustic communications. Trans. Emerg. Telecommun. Technol. **30**(12), e3712 (2019)
2. Ahmad, A.M., Barbeau, M., Garcia-Alfaro, J., Kassem, J., Kranakis, E., Porretta, S.: Doppler effect in the acoustic ultra low frequency band for wireless underwater networks. Mob. Netw. Appl. **23**(5), 1282–1292 (2018)
3. Ahmad, A.-M., Barbeau, M., Garcia-Alfaro, J., Kassem, J., Kranakis, E., Porretta, S.: Doppler effect in the underwater acoustic ultra low frequency band. In: Zhou, Y., Kunz, T. (eds.) Ad Hoc Networks. LNICST, vol. 223, pp. 3–12. Springer, Cham (2018). https://doi.org/10.1007/978-3-319-74439-1_1
4. Ahmad, A.-M., Barbeau, M., Garcia-Alfaro, J., Kassem, J., Kranakis, E., Porretta, S.: Low frequency mobile communications in underwater networks. In: Montavont, N., Papadopoulos, G.Z. (eds.) ADHOC-NOW 2018. LNCS, vol. 11104, pp. 239–251. Springer, Cham (2018). https://doi.org/10.1007/978-3-030-00247-3_22
5. Ahmed, R., Stojanovic, M.: Joint power and rate control for packet coding over fading channels. IEEE J. Oceanic Eng. **42**(3), 697–710 (2016)
6. Anjangi, P., Chitre, M.: Model-based data-driven learning algorithm for tuning an underwater acoustic link. In: 2018 Fourth Underwater Communications and Networking Conference (UComms), pp. 1–5. IEEE (2018)
7. Antonelli, G.: Underwater Robots. Springer Tracts in Advanced Robotics, vol. 96. Springer, Cham (2014). https://doi.org/10.1007/978-3-319-02877-4
8. Barbeau, M.: Weak signal underwater communications in the ultra low frequency band. In: Proceedings of the GNU Radio Conference, vol. 2, p. 8 (2017)
9. Barbeau, M., Blouin, S., Traboulsi, A.: Performance of an underwater communication system in a sea trial done in the Canadian Arctic. In: 2021 IEEE International Mediterranean Conference on Communications and Networking (MeditCom), pp. 448–453. IEEE (2021)
10. Button, R.W., Kamp, J., Curtin, T.B., Dryden, J.: A survey of missions for unmanned undersea vehicles. RAND National Defense Research Institute (2009)
11. Decarpigny, J., Hamonic, B., Wilson, O.: The design of low frequency underwater acoustic projectors: present status and future trends. IEEE J. Oceanic Eng. **16**(1), 107–122 (1991)
12. Defence Research and Development Canada: All Domain Situational Awareness (ADSA). Goverment of Canada, November 2016. https://www.canada.ca/content/dam/drdc-rddc/documents/en/adsa-program.pdf. Accessed 05 Mar 2021
13. Dol, H.S., Casari, P., van der Zwan, T., Otnes, R.: Software-defined underwater acoustic modems: historical review and the nilus approach. IEEE J. Oceanic Eng. **42**(3), 722–737 (2017)
14. Fano, R.: A heuristic discussion of probabilistic decoding. IEEE Trans. Inf. Theory **9**(2), 64–74 (1963)
15. Freitag, L., Partan, J., Koski, P., Singh, S.: Long range acoustic communications and navigation in the arctic. In: OCEANS 2015 - MTS/IEEE Washington, pp. 1–5, October 2015
16. Hixson, E.: A low-frequency underwater sound source for seismic exploration. J. Acoust. Soc. Am. **126**(4), 2234 (2009)
17. Jiang, Y.: A Practical Guide to Error-Control Coding Using Matlab. Artech House, Norwood (2010)

18. Kassem, J., Barbeau, M., Ahmad, A.M., Garcia-Alfaro, J.: GNU Radio blocks for long-lasting frames in mobile underwater acoustic communications. In: French GNU Radio Days, Lyon, France (2018). https://gnuradio-fr-18.sciencesconf.org/211038/document. Accessed 25 Feb 2019
19. Kassem, J., Barbeau, M., Ahmad, A.M., Garcia-Alfaro, J.: The implementation of GNU radio blocks for decoding long-lasting frames in mobile underwater acoustic communications. In: The Technical Proceedings of the 8th Annual GNU Radio Conference, Henderson, NV (2018). https://pubs.gnuradio.org/index.php/grcon/article/view/50. Accessed 25 Feb 2019
20. Massoud Salehi, P., Proakis, J.: Digital Communications. McGraw-Hill Education, New York (2007)
21. Otnes, R., Voldhaug, J.E., Haavik, S.: On communication requirements in underwater surveillance networks. In: OCEANS 2008-MTS/IEEE Kobe Techno-Ocean, pp. 1–7. IEEE (2008)
22. Otnes, R., et al.: Underwater Acoustic Networking Techniques. Springer, Heidelberg (2012). https://doi.org/10.1007/978-3-642-25224-2
23. Proakis, J., Salehi, M.: Digital Communication, 5th edn. McGrah-Hill Higher Education, New York (2008)
24. Radosevic, A., Ahmed, R., Duman, T.M., Proakis, J.G., Stojanovic, M.: Adaptive OFDM modulation for underwater acoustic communications: design considerations and experimental results. IEEE J. Oceanic Eng. **39**(2), 357–370 (2013)
25. Song, A., Stojanovic, M., Chitre, M.: Editorial underwater acoustic communications: where we stand and what is next? IEEE J. Oceanic Eng. **44**(1), 1–6 (2019)
26. Stojanovic, M.: On the relationship between capacity and distance in an underwater acoustic communication channel. SIGMOBILE Mob. Comput. Commun. Rev. **11**(4), 34–43 (2007)
27. Traboulsi, A., Barbeau, M.: Oceanus (2021). https://github.com/ahmadtraboulsi/oceanus
28. Wan, L., et al.: Adaptive modulation and coding for underwater acoustic OFDM. IEEE J. Oceanic Eng. **40**(2), 327–336 (2014)
29. Wikipedia: Underwater locator beacon (2018). https://en.wikipedia.org/wiki/-Underwater_locator_beacon